The geometry related to the IN and OUT situations for multiple GIXD is also important to understand the phase effect on the surface-reflected intensities. As shown in Figs. 5 and 11, the sense of asymmetry of P_0^s and P_h^s for the IN situation is the reverse of that for the OUT situation. This is similar to the geometric effect on the intensity of a three-beam diffraction from a crystal bulk (Chang, 1982).

It is also worth noting that for the strong primary reflection like the 220 in the case $(000)(220)(202)/(02\bar{2})$, the P_{220}^s near ψ_3 is much weaker than the P_{220}^s for $\psi < \psi_3$, while for the weak primary reflection 222, the P_{222}^s at ψ_3 and especially at θ_1 has much higher intensity than the usual two-beam (222) GIXD intensity. As ψ_3 is closer to θ_1, the peak intensity P_{222}^s increases in order of magnitude. These two situations resemble the *Aufhellung* and *Umweganregung*, respectively, in ordinary multiple diffractions from bulk crystals (Renninger, 1937).

As has been demonstrated, both surface *Aufhellung* and *Umweganregung* seem to be useful in centric phase determination from the detection of the surface-reflected intensity variation.

The authors are indebted to the National Science Council for financial support under grant NSC 79-0204-M007-05. One of us, TPT, thanks the same organization for providing a graduate fellowship during the course of this study and H. H. Hung for useful discussions.

References

AFANAS'EV, A. M. & MELKONYAN, M. K. (1983). *Acta Cryst.* A**39**, 207-210.
CHANG, S. L. (1982). *Phys. Rev. Lett.* **48**, 163-166.
CHANG, S. L. & TANG, M. T. (1988). *Acta Cryst.* A**44**, 1065-1072.
CHAPMAN, L. D., YODER, D. R. & COLELLA, R. (1981). *Phys. Rev. Lett.* **46**, 1578-1581.
COLELLA, R. (1974). *Acta Cryst.* A**30**, 413-423.
COWAN, P. L. (1985). *Phys. Rev. B*, **32**, 5437-5439.
DURBIN, S. M. & GOG, T. (1989). *Acta Cryst.* A**45**, 132-141.
FUOSS, P. H., LIANG, K. S. & EISENBERGER, P. (1989). *Synchrotron Radiation Research: Advances in Surface Science*, edited by R. Z. BACHRACH. New York: Plenum.
HART, M. & LANG, A. R. (1961). *Phys. Rev. Lett.* **7**, 120-121.
HOCHE, H. R., BRÜMMER, O. & NIEBER, J. (1986). *Acta Cryst.* A**42**, 585-587.
HØIER, R. & AANESTAD, A. (1981). *Acta Cryst.* A**37**, 787-794.
HÜMMER, K. & BILLY, H. W. (1986). *Acta Cryst.* A**42**, 127-133.
HÜMMER, K., WECKERT, E. & BONDZA, H. (1989). *Acta Cryst.* A**45**, 182-187.
HUNG, H. H. & CHANG, S. L. (1989). *Acta Cryst.* A**45**, 823-833.
International Tables for X-ray Crystallography (1974). Vol. IV. Birmingham: Kynoch Press. (Present distributor Kluwer Academic Publishers, Dordrecht.)
JURETSCHKE, H. J. (1982). *Phys. Rev. Lett.* **48**, 1487-1489.
KAMBE, K. & MIYAKE, S. (1954). *Acta Cryst.* 7, 218-219.
MARRA, W. C., EISENBERGER, P. & CHO, A. Y. (1979). *J. Appl. Phys.* **50**, 6927-6933.
MO, F., HAUBACH, B. C. & THORKILDSEN, G. (1988). *Acta Chem. Scand. Ser. A*, **42**, 130-138.
POST, B. (1977). *Phys. Rev. Lett.* **39**, 760-763.
RENNINGER, M. (1937). *Z. Phys.* **106**, 141-176.
SAKATA, O. & HASHIZUME, H. (1988). *Jpn. J. Appl. Phys.* **27**, L1976-L1979.
SHEN, Q. & COLELLA, R. (1988). *Acta Cryst.* A**44**, 17-21.
VINEYARD, G. H. (1982). *Phys. Rev. B*, **26**, 4146-4159.

Acta Cryst. (1990). A**46**, 576-584

The Intensity Distribution Observed with a Multi-Crystal X-ray Diffractometer

BY E. L. GARTSTEIN

Department of Physics, University of Edinburgh, Mayfield Road, Edinburgh EH9 3JZ, Scotland, and Neeve Shaanan, Str. Berl Katzenelson 56/4, Haifa, Israel

AND R. A. COWLEY

Department of Physics, University of Edinburgh, Mayfield Road, Edinburgh EH9 3JZ, Scotland, and Clarendon Laboratory, University of Oxford, Parks Road, Oxford, England

(*Received* 17 *October* 1989; *accepted* 17 *March* 1990)

Abstract

Expressions are obtained for the intensity distributions which are observed when Bragg reflections are studied using an X-ray multi-crystal diffractometer. The expressions are obtained for both Bragg and Laue geometry at the sample, and assuming that the monochromator, sample and analyser elements are all perfect crystals. Detailed calculations are made of several configurations with both laboratory-based and synchrotron sources, and the results are compared with experimental measurements. The comparison shows that the theory gives reliable results not only for the half-widths of the distributions, but also for the tails of the distributions resulting from the dynamical effects in one or more of the crystals.

0108-7673/90/070576-09$03.00

I. Introduction

The multi-crystal X-ray diffractometer is a powerful instrument for the study of X-ray scattering when high momentum resolution is required. High momentum resolution enables the separation of the Bragg and the diffuse scattering, and this is of importance in X-ray studies of phase transitions (*e.g.* Andrews & Cowley, 1986), surfaces and interfaces (Andrews & Cowley, 1985; Cowley & Ryan, 1987), imperfections (Zaumseil & Winter, 1982) and magnetic scattering (Gibbs, Moreton, d'Amico, Bohr & Grier, 1985; Goldman *et al.*, 1987). It is clear that a detailed knowledge of the intensity distribution around the Bragg reflections is essential if these experiments are to be optimized and interpreted reliably. The calculations reported below were performed to show that the intensity distributions can indeed be reliably calculated, and to present the results for a variety of different configurations.

Calculations of the resolution function of a triple-crystal X-ray diffractometer have been performed by Zaumseil & Winter (1982), but they considered only a non-dispersive arrangement and identical scattering planes for monochromator, sample and analyser crystals. The central part of the resolution was also calculated by Pynn, Fujii & Shirane (1983) and their approach was to use the procedure developed by Bjerrum-Möller & Nielsen (1969) for the neutron triple-axis spectrometer. In the present paper we extend these results to the more general case of a multi-crystal X-ray diffractometer with, in principle, different materials for each of the crystals, and we calculate the intensities not only in the centre but also in the wings of the distributions. The principle of the calculations has been outlined (Lucas, Gartstein & Cowley, 1989), but in this paper there is a more detailed description of the method and it is generalized to more complex situations.

II. The intensity distribution for an X-ray diffractometer

In this section we describe the calculation of the X-ray intensity distribution observed when the diffractometer is scanned around the Bragg reflection of a perfect sample crystal. The scattering is assumed to arise from a perfect-crystal monochromator and analysing elements (Fig. 1), and we assume that the reflectivity of each element is given by the dynamical theory of X-ray diffraction. A typical triple-crystal diffractometer is shown schematically in Fig. 1 and the intensity around a Bragg lattice point, Q_s, is obtained by scanning the sample orientation ψ and angle φ through which the X-rays are scattered. The deviations of the wavevector transfer from the reciprocal-lattice vector are then given by

$$q_\parallel = [(2\pi/\lambda)\sin\theta_s](2\Delta\psi - \Delta\varphi) \qquad (2.1)$$

$$q_\perp = [(2\pi/\lambda)\cos\theta_s](\Delta\varphi) \qquad (2.2)$$

where $\Delta\psi$ and $\Delta\varphi$ are the deviations of the two angles from their Bragg settings and $\theta_s = \varphi/2$ is the Bragg angle. For small changes in angle, rotation of the analyser crystal is equivalent to a change in φ, as shown in Fig. 1.

In calculating the intensity as a function of $q_\parallel$ and $q_\perp$ the divergence of the beams perpendicular to the scattering plane have been neglected. This is because the perpendicular divergence is relatively easier to calculate, and is largely uncoupled from the in-plane divergence (Cowley, 1987). There is a slight effect because the diffraction angle is effectively changed by $\gamma^2/2\tan\theta_s$, where γ is the vertical divergence, and so we are assuming that γ is sufficiently small that this effect is negligible.

Following the analysis of Zachariasen (1975), the intensity observed in a complex instrument with m crystal components for the monochromator and n crystal components for the analyser is given by the convolution integral

$$I(\Delta\psi, \Delta\varphi) = \int_{-\infty}^{\infty}\int_{-\infty}^{\infty} J(\Delta\lambda)F(\alpha)R_{M_1}(\Delta\theta_{M_1}) \times R_{M_2}(\Delta\theta_{M_2})\ldots R_{M_m}(\Delta\theta_{M_m})R_s(\Delta\theta_s) \times R_{A_1}(\Delta\theta_{A_1})\ldots R_{A_n}(\Delta\theta_{A_n})\,\mathrm{d}\alpha\,\mathrm{d}\lambda, \qquad (2.3)$$

where M, s and A denote monochromator, sample and analyser respectively.

$J(\Delta\lambda)$ is the wavelength distribution around the nominal wavelength λ. For an X-ray tube the characteristic line is well described by a Lorentzian

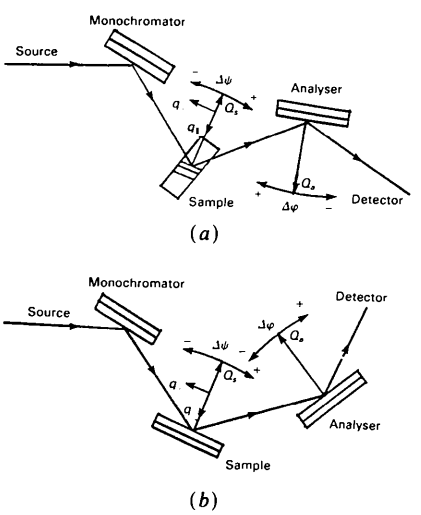

(*a*) (*b*)

Fig. 1. (*a*) Triple-crystal arrangement (+1 −1 +1) with a sample in Laue geometry. $\Delta\psi$ and $\Delta\varphi$ are the angular deviations around the setting angle ψ for the sample and the scattering angle φ. (*b*) Triple-crystal arrangement (+1 −1 −1) with a sample in Bragg geometry.

distribution

$$J(\Delta\lambda) = \sigma/[(\Delta\lambda)^2 + \sigma^2], \qquad (2.4)$$

where for the Cu $K\alpha_1$ line $\sigma = 5{\cdot}8 \times 10^{-4}$ Å. For a synchrotron source, $J(\Delta\lambda)$ can frequently be taken as effectively a constant within the relevant range of $\Delta\lambda$. The angular divergence, α, before the monochromator for an X-ray tube is typically much larger than the other resolution elements, while for a synchrotron $F(\alpha)$ is determined either by the emission profile of the synchrotron or by the slits introduced prior to the monochromator.

Zachariasen (1945) calculated the reflectivity of a monochromator and sample for a ray with wavelength $\lambda + \Delta\lambda$ and angular deviation α from the direction of the nominal ray with wavelength λ. We have extended his calculation for the more general system considered here in which the beam is deflected at each element to the left (−1) or right (+1) as defined by the parameters n_{M-K}, n_s or n_{AK}. The results are

$$\begin{aligned}
\Delta\theta_{M_1} &= \alpha - (\Delta\lambda/\lambda)\tan\theta_{M_1} \\
\Delta\theta_{M_2} &= (\Delta\lambda/\lambda)\tan\theta_{M_2} - n_{M_1}n_{M_2} \\
&\quad \times[(\Delta\lambda/\lambda)\tan\theta_{M_1} - b_{M_1}\Delta\theta_{M_1}] \\
\Delta\theta_{M_m} &= -(\Delta\lambda/\lambda)\tan\theta_{M_m} - n_{M_{m-1}}n_{M_m} \\
&\quad \times[(\Delta\lambda/\lambda)\tan\theta_{M_{m-1}} - b_{M_{m-1}}\Delta\theta_{M_{m-1}}], \qquad (2.5)
\end{aligned}$$

while for the sample

$$\begin{aligned}
\Delta\theta_s &= (\Delta\lambda/\lambda)\tan\theta_s - \Delta\psi - n_s n_{M_m} \\
&\quad \times[(\Delta\lambda/\lambda)\tan\theta_{M_m} - b_{M_m}\Delta\theta_{M_m}], \qquad (2.6)
\end{aligned}$$

and for the analyser

$$\begin{aligned}
\Delta\theta_{A_1} &= -(\Delta\lambda/\lambda)\tan\theta_{A_1} - n_{A_1}n_s \\
&\quad \times[\Delta\varphi - \Delta\psi + (\Delta\lambda/\lambda)\tan\theta_s - b_s\Delta\theta_s], \\
\Delta\theta_{A_2} &= -(\Delta\lambda/\lambda)\tan\theta_{A_2} - n_{A_2}n_{A_1} \\
&\quad \times[(\Delta\lambda/\lambda)\tan\theta_{A_1} - b_{A_1}\Delta\theta_{A_1}]. \qquad (2.7)
\end{aligned}$$

In these expressions the angular offset of any element from the Bragg condition, $\Delta\psi$ or $\Delta\varphi$ in this case, occurs in the expression for the angular deviation in the crystal components which are later in the system. We have assumed that all of the components of the monochromator and analyser are perfectly aligned. If this is not the case the expressions are readily obtained within the same formalism including the appropriate mis-sets. The parameters b_{M_1} *etc.* are the parameters b occurring in the general case of asymmetric Bragg reflection

$$b = \sin(\beta - \theta)/\sin(\beta + \theta), \qquad (2.8)$$

where β is the angle between the surface of the crystal and the reflecting planes, and is positive when the angle between the incident beam and the crystal surface is less than the Bragg angle. For symmetric reflections in Bragg geometry (reflectivity) $b = -1$ and in Laue geometry (transmission) $b = +1$.

The reflectivity of perfect crystals with extended-face Bragg geometry was derived by Cole & Semple (1962) for non-centrosymmetric crystals. We have used their expression for the reflectivity of the monochromator and analyser elements, and for the samples

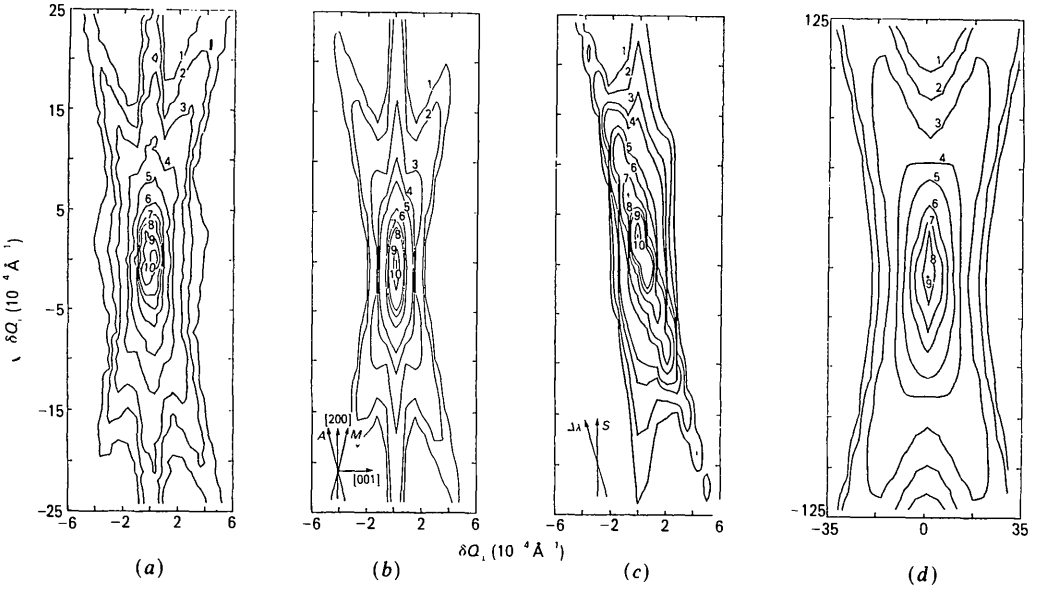

Fig. 2. (*a*) Measured intensity distribution near InP 200 Bragg reflection in (+1 −1 +1) arrangement. Intensity contour levels are given with respect to the intensity maximum I_0: $I/I_0 = (1)\ 10^{-3}$; (2) 2×10^{-3}; (3) 6×10^{-3}; (4) $1{\cdot}2\times10^{-2}$; (5) 5×10^{-2}; (6) 0·1; (7) 0·2; (8) 0·5; (9) 0·7; (10) 0·9. (*b*) Simulated intensity distribution near InP 200 in (+1 −1 +1) arrangement. Intensity contour levels as in (*a*). (*c*) Simulated intensity distribution near InP 200 in (+1 −1 +1) arrangement. Intensity contour levels are the same as in (*a*). (*d*) Simulated resolution function for InP 200 Bragg reflection in (+1 −1 +1) arrangement. Intensity contour levels are $I/I_0 = (1)\ 10^{-3}$; (2) 2×10^{-3}; (3) 9×10^{-3}; (4) 5×10^{-2}; (5) 0·1; (6) 0·5; (7) 0·7; (8) 0·9; (9) 1.

in Bragg geometry, including the effects of the beam polarization and the real and imaginary parts of the structure factor. When the sample was in Laue geometry the function $R_s(\theta)$ was taken from Zachariasen (1945) including the effect of the thickness of the sample, t, and the linear absorption coefficient.

In discussing the resolution of the instrument for measuring diffuse scattering it is convenient to replace $R_s(\theta)$ by $\delta(\theta)$. When this is done the full theory can be compared with the approximate analytic theory developed earlier (Cowley, 1987).

III. Calculations and comparison with experiment

1. *Rotating-anode source and Bragg geometry*

A triple-crystal X-ray diffractometer was used (Lucas *et al.*, 1989) with perfect single crystals of germanium as both monochromator and analyser. Both were aligned for the symmetric 111 Bragg reflection in the Bragg geometry, and a (1, −1, 1) geometry for the scattering senses was used. The source was Cu $K\alpha$ radiation from a rotating-anode generator operating at 2·7 kW, and a slit immediately before the sample was used to eliminate the $K\alpha_2$ line in the emitted X-ray spectrum. A slit of 0·25 mm was used perpendicular to the scattering plane. The sample was a perfect InP crystal with the surface normal [100] and the [010] direction in the scattering plane. The data were collected by scanning $q_\parallel$ and $q_\perp$ close to the Bragg reflections from which a contour map of the scattered intensity was constructed.

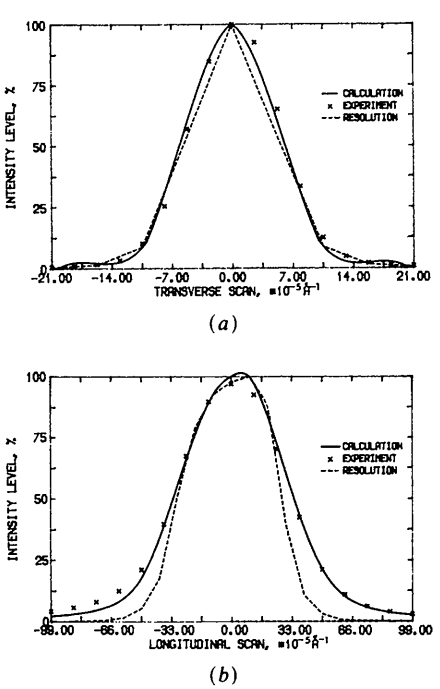

Fig. 3. (*a*) Calculated experimental and resolution transverse scans for the InP 200 Bragg reflection. (*b*) Calculated, experimental and resolution longitudinal scans for InP 200 Bragg reflection.

Table 1. *Comparison of the resolution function in Bragg geometry calculated, with the Gaussian theory (Cowley, 1987), and experimental*

FWHM × 10^{-5} Å^{-1}.

Reflection		Transverse	Longitudinal
200	Calculation	10·1	58
	Gaussian	11·7	43
	Experiment	10·0 (5)	55 (1)
420	Calculation	27	117
	Gaussian	25	115
	Experiment	29 (1)	112 (5)

The measured intensity pattern is shown in Fig. 2(*a*) for the symmetrical 200 Bragg reflection. The result of the corresponding calculation of the intensity profile without any adjustable parameters is shown in Fig. 2(*b*). Clearly there is a very reasonable agreement between the experiment and theory as to the shape of the scattering and the intensity. The shape of the pattern can be understood as explained by Ryan (1986) and by Lucas *et al.* (1989). For perfect crystals the reflectivities have long $(\Delta\theta)^{-2}$ tails, which means that there are much longer tails to the reflectivity functions than if they were Gaussians. The streaks then arise when any two of the three crystal reflectivities have zero argument. The streak corresponding to the monochromator occurs at an angle of $-\varphi/2$ to the wavevector transfer, the streak from the analyser at $\varphi/2$, and the streak from the sample is perpendicular to the extended surface. All of these three streaks are clearly present in Figs 2(*a*) and (*b*). Fig. 2(*d*) shows the calculation of the resolution function of the instrument $R_s(\theta) = \delta(\theta)$, and this is clearly similar to Figs. 2(*a*) and (*b*), except that the central streak due to the sample surface is missing. Fig. 3 compares the calculated and measured resolution function in the centre of the scan by showing the scans longitudinally and transversely through the centre. The results are in very good agreement with one another and are compared with the corresponding results for the Gaussian approximate theory in Table 1. In comparing Figs. 2(*a*) and (*b*) the main discrepancy is in the bulge appearing for low-intensity contours in the centre of the pattern whereas the calculated pattern shows no such bulge. This discrepancy arises because the calculations neglect the thermal diffuse scattering, and this is strongest for small $q_\perp$, $q_\parallel = 0$, owing to the transverse acoustic phonons.

The 200 InP reflection has nearly the same Bragg angle as the 111 Ge reflection and so the wavelength dispersion has only a very small effect in the (1, −1, 1) configuration. This is illustrated in Fig. 2(*c*) where we calculate the intensity which would be observed in the (1, −1, −1) geometry; clearly the pattern is very different from Figs. 2(*a*) and (*b*).

A similar set of experiments and calculations were performed for the asymmetric 420 reflection as shown in Figs. 4(*a*) and (*b*) and Table 1. The streak along the [420] direction corresponds to the wavelength spread, while that along the direction labelled *M* arises from the monochromator, and the analyser streak and surface streak are perpendicular to the surface of the InP and along the [100] direction. Fig. 4 and Table 1 show clearly that experiment and calculation are in very reasonable accord for the general shape of the intensity, and are in quantitative agreement for the widths of the central region.

2. *Rotating-anode source and Laue geometry*

The X-ray diffractometer was the same as for the measurements with the sample in Bragg geometry except that the slit perpendicular to the scattering plane was increased to 4 mm. An InP sample was used in Laue geometry and was 0·04 mm thick, so

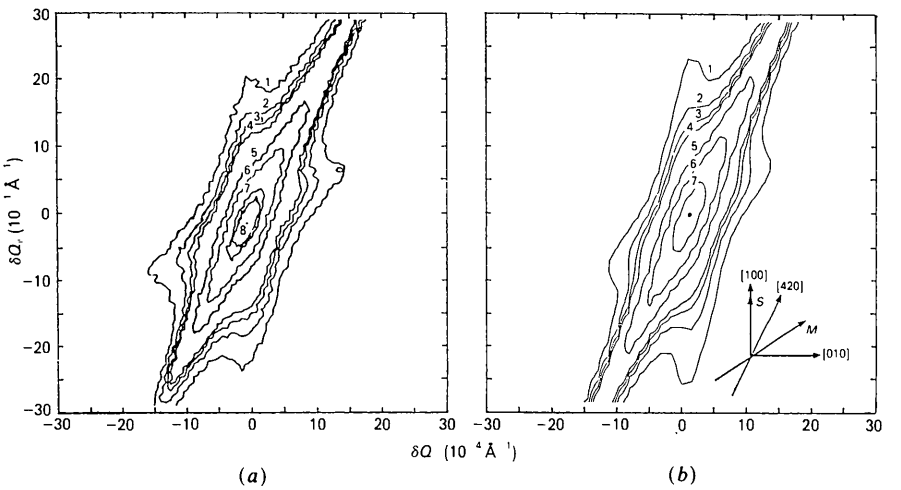

Fig. 4. (*a*) Measured intensity distribution near InP 420 Bragg reflection in (+1 −1 +1) arrangement. Intensity contour levels: I/I_0 = (1) $2{\cdot}5\times10^{-3}$; (2) 5×10^{-3}; (3) $7{\cdot}5\times10^{-3}$; (4) 10^{-2}; (5) 5×10^{-2}; (6) 0·1; (7) 0·5; (8) 1. (*b*) Simulated intensity distribution for InP 420 in (+1 −1 +1) arrangement. The intensity contour levels are the same as in (*a*).

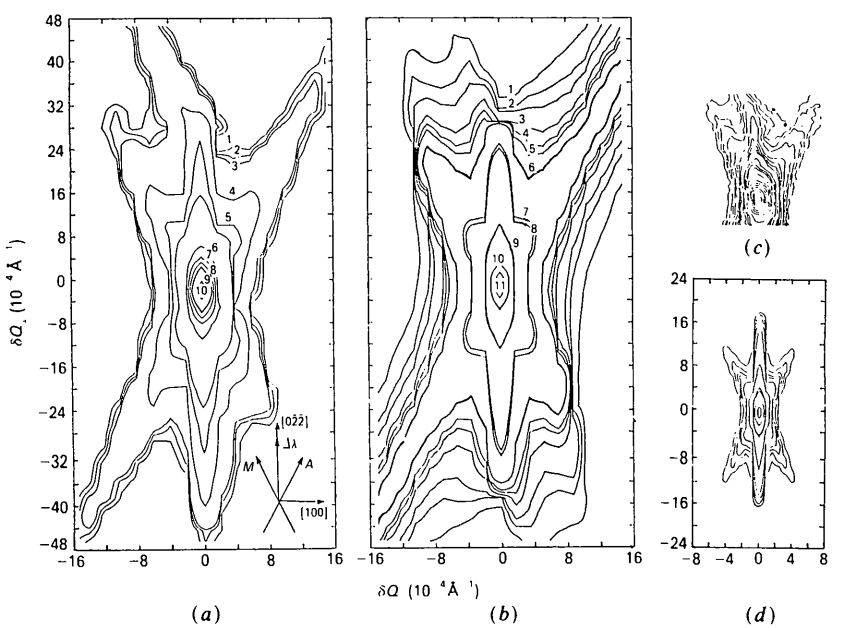

Fig. 5. (*a*) Measured intensity distribution near InP 0$\bar{2}\bar{2}$ Laue reflection in (+1 −1 +1) arrangement. Intensity contour levels: I/I_0 = (1) 3×10^{-4}; (2) 4×10^{-4}; (3) 10^{-3}; (4) 3×10^{-3}; (5) 10^{-2}; (6) 0·1; (7) 0·2; (8) 0·3; (9) 0·5; (10) 0·75. (*b*) Simulated intensity distribution near InP 0$\bar{2}\bar{2}$ Laue reflection in (+1 −1 +1) arrangement. Intensity contour levels: I/I_0 = (1) 2×10^{-5}; (2) 4×10^{-5}; (3) 2×10^{-4}; (4) 3×10^{-4}; (5) 5×10^{-4}; (6) 10^{-3}; (7) 10^{-2}; (8) 5×10^{-2}; (9) 0·1; (10) 0·5; (11) 0·75. (*c*) Insert showing measured intensity distribution near 0$\bar{2}\bar{2}$ Laue reflection with a small step scan. Streak due to the wavelength dispersion is gradually changing its direction. (*d*) Simulated resolution function for InP 0$\bar{2}\bar{2}$ Laue reflection. Intensity contour levels are the same as for (*b*).

Table 2. *Comparison of the experimental and calculated results for the sample in Laue geometry*

Reflection	Experiment (FWHM × 10^{-5} Å^{-1}) Transverse	Experiment (FWHM × 10^{-5} Å^{-1}) Longitudinal	Calculation (FWHM × 10^{-5} Å^{-1}) Transverse	Calculation (FWHM × 10^{-5} Å^{-1}) Longitudinal	Resolution (FWHM × 10^{-5} Å^{-1}) Transverse	Resolution (FWHM × 10^{-5} Å^{-1}) Longitudinal
$0\bar{2}\bar{2}$	25 (2)	56 (5)	18	54	14	54
$1\bar{1}\bar{1}$	18·5 (2)	49 (5)	13	47	11	38

that the absorption parameter $\mu t = 44$. The slab normal was the [100] direction and the [011] direction was aligned in the scattering plane. The scattering observed near the symmetrical $0\bar{2}\bar{2}$ Bragg reflection is shown in Fig. 5(*a*). As in the case of Bragg reflection the monochromator and analyser streaks are at $-\varphi/2$ and $\varphi/2$ to the wavevector transfer, and the streak due to the wavelength spread is along the wavevector transfer. Fig. 5(*b*) shows the calculated distribution of intensity; very reasonable agreement is observed. The widths of the central part of the scattering are given in Table 2. The resolution function for the same scattering conditions is shown in Fig. 5(*d*) and the pattern is fairly similar, showing that the sample is

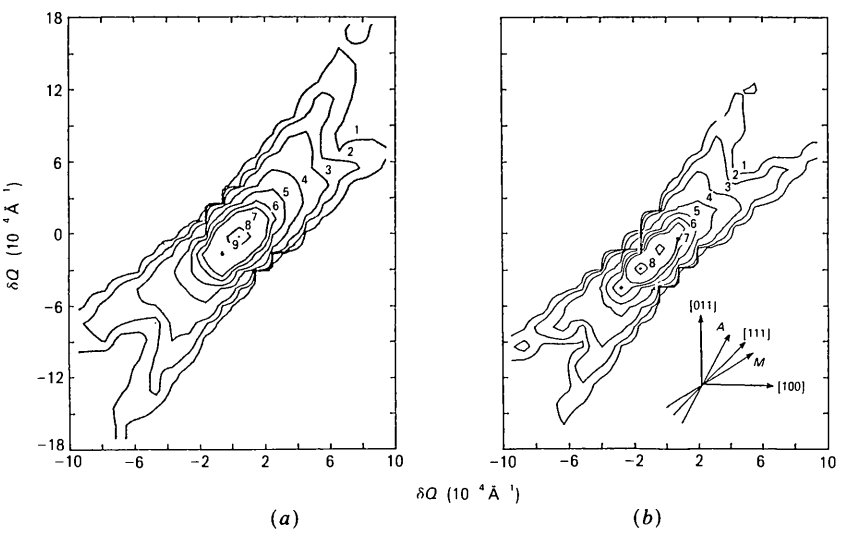

Fig. 6. (*a*) Measured intensity distribution near InP $1\bar{1}\bar{1}$ Laue reflection in (+1 −1 +1) arrangement. Intensity contour levels: I/I_0 = (1) 3×10^{-3}; (2) 6×10^{-3}; (3) $1{\cdot}2\times10^{-2}$; (4) 5×10^{-2}; (5) 0·1; (6) 0·2; (7) 0·5; (8) 0·75; (9) 1. (*b*) Simulated intensity distribution near InP $1\bar{1}\bar{1}$ Laue reflection in (+1 −1 +1) arrangement. Intensity contour levels are the same as for (*a*). The detailed structure is due to the computational procedure.

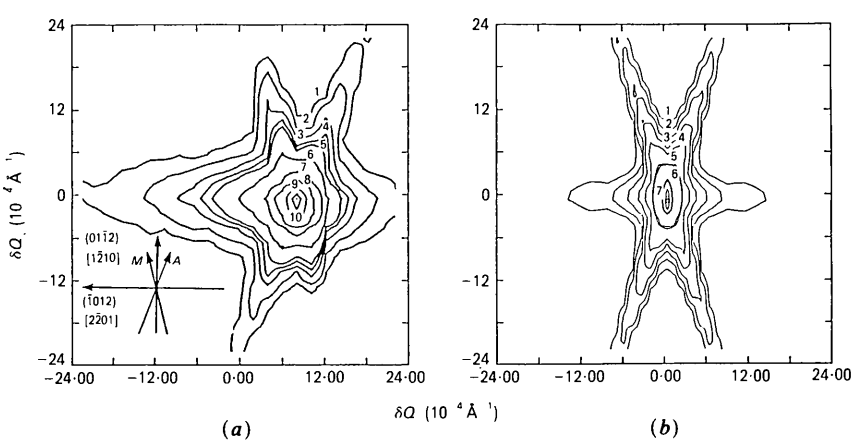

Fig. 7. (*a*) Measured intensity distribution near sapphire $01\bar{1}\bar{2}$ Laue reflection in (+1 −1 +1) arrangement. Intensity contour levels: I/I_0 = (1) 5×10^{-4}; (2) 10^{-3}; (3) 2×10^{-3}; (4) 5×10^{-3}; (5) 10^{-2}; (6) 5×10^{-2}; (7) 0·1; (8) 0·5; (9) 0·7; (10) 0·9. (*b*) Simulated intensity distribution near sapphire $01\bar{1}\bar{2}$ Laue reflection in (+1, −1, +1) arrangement. Intensity contour levels: I/I_0 = (1) 5×10^{-4}; (2) 10^{-3}; (3) 2×10^{-3}; (4) 5×10^{-3}; (5) 10^{-2}; (6) 2×10^{-2}; (7) 0·5; (8) 0·75.

having little effect on the scattered distributions. One difference, however, is the bending of the $\Delta\lambda$ streak for $q_{\|}$ positive in Figs 5(*a*), (*b*) and (*c*). Since the bending is absent in the calculated resolution function it must arise from an interaction between the sample and the resolution, but we have not as yet understood the result in detail. It is, however, well reproduced by the calculations (Fig. 5*b*).

A similar comparison is shown for the distributions obtained around the asymmetric $1\bar{1}\bar{1}$ reflection in Figs. 6(*a*) and (*b*). For this reflection the Bragg angles of all the crystals are similar and so the $\Delta\lambda$ dispersion is negligible. The two streaks arise from the monochromator and analyser as shown in Fig. 6(*b*). Clearly the agreement between experiment and calculation for these reflections is reasonably satisfactory, apart from the fact that the experimental curves are wider than the theoretical ones in the $q_{\perp}$ direction (Table 2). This could arise from the introduction of defects into the InP sample when it was thinned down to make the Laue sample.

The effect of the sample thickness was studied by examining the $01\bar{1}\bar{2}$ reflection of sapphire. The sample had a thickness of 0·4 mm when $\mu t = 0{\cdot}8$. The results (Fig. 7) are quite different from those of the InP $0\bar{2}\bar{2}$ reflection (Fig. 5). This is because the surface streak is in this case perpendicular to the reflecting planes and is clearly visible although suppressed by the large μt of the InP, and in contrast the Δt streak is absent for the sapphire because the Bragg angle is close to that of the monochromator and analyser, giving non-dispersive conditions. The symmetry of the surface streak in the experiment is because there was 0·25 μm of epitaxically grown Si on the sapphire, but a study of the effect of this on the scattering will be reported elsewhere. The calculations for the intensity profile (Fig. 7*b*) give a very similar pattern to the measurements except that no account is taken of the Si layer and so the surface streak is symmetrical in the calculations.

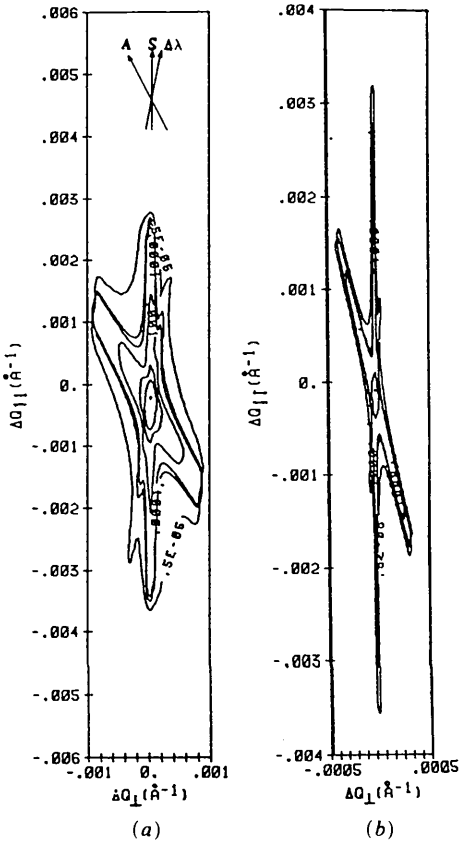

(*a*) (*b*)

Fig. 8. (*a*) Simulated intensity distribution for the wavelength $\Delta\lambda = 1{\cdot}38$ Å around the 400 Si symmetrical Bragg reflection. Directions of the analyser, surface and wavelength dispersion streaks are denoted by *A*, *S* and $\Delta\lambda$, respectively. The intensity contour levels correspond to I/I_{max}. (*b*) Analogous simulation for the wavelength $\lambda_0 = 0{\cdot}62$ Å.

3. *Synchrotron source and Bragg geometry*

These calculations were performed in such a way as to be similar to typical conditions of experiments performed at the Daresbury SRS on station 9.4. A channel-cut silicon double monochromator was used, with a silicon single-bounce analyser and a silicon sample. The 111 reflections were used for the mono-

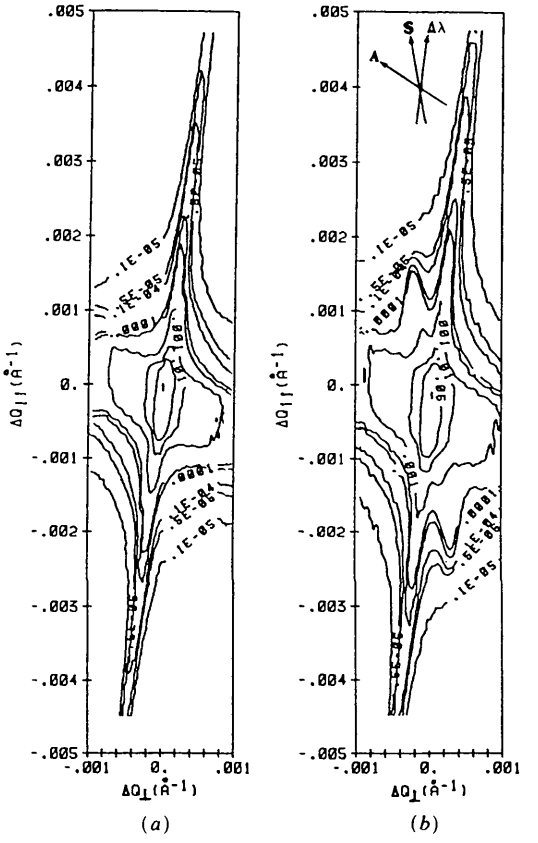

(*a*) (*b*)

Fig. 9. (*a*) Simulated intensity distribution around asymmetrical 711 Si Bragg reflection. (*b*) Analogous simulation around $7\bar{1}\bar{1}$ Si Bragg reflection. Notation as in Fig. 8.

chromator and analyser and the sample had a surface perpendicular to the [100] direction, while the [011] direction was in the scattering plane. The calculations were performed by taking $J(\lambda)$ as a constant around the nominal wavelength λ_0 and the pre-monochromator collimation as $1{\cdot}3\times10^{-5}$ rad. The intensity distributions for the symmetrical 400 Bragg reflection are shown in Fig. 8 for incident wavelengths of 1·38 and 0·62 Å. The patterns clearly show the sample surface streak but unlike the case of the InP 200 reflection the pattern is asymmetric (Fig. 2). In part this is caused by the double monochromator, because this produces a tail proportional to $(\Delta\theta)^{-4}$ which effectively suppresses the monochromator streak. The analyser streak is, however, still clearly seen. The other differences arise because the effect of the wavelength spread is different from that on a conventional source, since the collimation before the monochromator is very good. A straightforward calculation shows that the $\Delta\lambda$ streak occurs at an angle to the wavevector transfer of

$$\tan^{-1}\left(\frac{\tan\theta_A\tan\theta_s}{2\tan\theta_s-\tan\theta_A}\right). \qquad (3.1)$$

In Fig. 8 the effect of the wavelength spread can just be seen separately from the sample surface streak. Measurements at the SRS at the Daresbury Laboratory (Lucas, 1989) of the half-width of the 400 Bragg reflection in silicon yield $1{\cdot}5(2)\times10^{-4}$ Å^{-1} parallel to Q and $0{\cdot}5(1)\times10^{-4}$ Å^{-1} perpendicular to Q, whereas the calculated results are $1{\cdot}7\times10^{-4}$ and $0{\cdot}4\times10^{-4}$ Å^{-1} respectively.

Figs. 9(a) and (b) show similar calculations with $\lambda_0=1{\cdot}38$ Å for the 711 and $7\bar{1}\bar{1}$ reflections. The $\Delta\lambda$ and analyser streaks are clearly seen, and in Fig. 9(b) the surface streak is also visible. In Fig. 9(a) the surface streak is obscured by the $\Delta\lambda$ streak. In Figs. 9(a) and (b) it is clear that the central part of the resolution function is not aligned along the wavevector transfer. This is different from the case of a conventional source (Cowley, 1987).

Equation (3.1) shows that the wavelength streak is perpendicular to the wavevector transfer if $\tan\theta_s=\frac{1}{2}\tan\theta_A$. This effect has been calculated by assuming that the monochromator and analyser are symmetric 222 InP reflections while the sample reflection is a symmetric 111 InP reflection. The results are shown in Fig. 10(a). The $\Delta\lambda$ streak is barely visible but there are strong analyser and sample surface streaks. Finally, a similar simulation was calculated for a

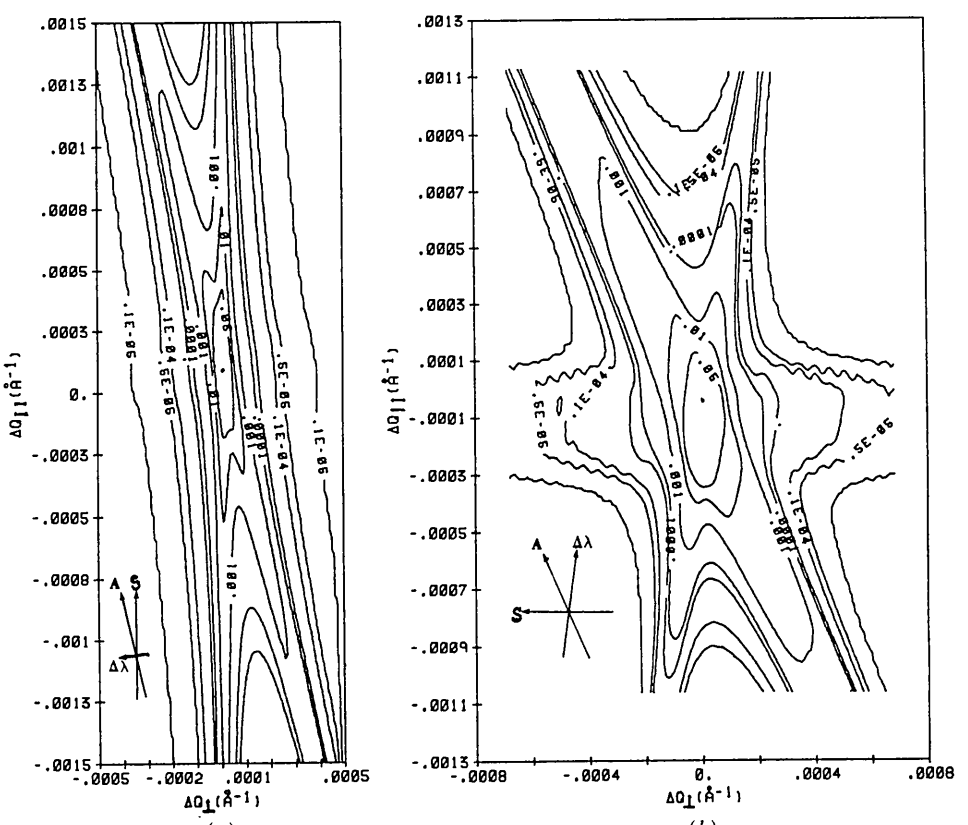

Fig. 10. (a) Simulated intensity distribution around 111 InP symmetrical Bragg reflection with the 222 InP symmetrical Bragg reflections from the monochromator and the analyser. Notation as in Fig. 8. (b) Simulated intensity distribution around $0\bar{2}\bar{2}$ Si symmetrical Laue reflection. Notation as in Fig. 8.

symmetric 022 Si reflection in Laue geometry. In this case, as in § III.2, the sample surface streak is perpendicular to the wavevector transfer and there are strong analyser and $\Delta\lambda$ streaks (Fig. 10*b*).

IV. Summary and concluding remarks

The intensity profiles of the Bragg reflections measured with an X-ray diffractometer have been calculated in detail. A general formalism has been developed which can be used for either conventional sources or synchrotron sources and can be used for multi-element monochromators and analysers. Detailed calculations down to the 10^{-4} level have been made for conventional sources with single-bounce monochromators and analysers with the sample in both Bragg and Laue geometry. The results are in generally good agreement with experiment and give a good account of the streaks in reciprocal space arising from the long tails of the non-Gaussian reflectivity profiles.

The calculations have also been performed for a double monochromator and a synchrotron source. Unfortunately we do not have available detailed measurements with which to compare the results of the calculations. We conclude, however, that the analysis presented here does give a very adequate description of the resolution function of X-ray diffractometers, and enables experiments to be more fully optimized. An example of this is the use of asymmetrically cut monochromators and analysers as used by Pick, Bickmann, Pofahl, Zwall & Wenzl (1977). The theory (Kikuta & Kohra, 1970) shows that the angular width of the incident and scattered beams from an asymmetrically cut crystal are

$$\omega_i = \omega_s/|b|^{1/2}, \quad \omega_f = \omega_s|b|^{1/2},$$

where ω_s is the width of the reflection for the same reflection from a symmetrically cut crystal. With these results the angular acceptance range can be increased and the emergence range decreased, giving improved resolution and increased intensity. A simulation of this effect was performed for Ge(111) reflecting planes inclined at 11° to the (111) surface of the crystal when $b_M = -0{\cdot}11$ and $b_A = 1/b_M$. The calculated half-widths are then given for a sample of InP in both Bragg and Laue geometry in Table 3. The intensity maxima in both cases were also increased by a factor of about three.

Table 3. *The calculated resolution function for asymmetric monochromator and analyser*

The corresponding resolutions for symmetrically cut crystals are in parentheses.

Resolution	Transverse (FWHM $\times 10^{-5}$ Å^{-1})	Longitudinal (FWHM $\times 10^{-5}$ Å^{-1})
InP 200 Bragg geometry	6·2 (10·1)	20·7 (58)
InP $0\bar{2}\bar{2}$ Laue geometry	9·5 (18)	18 (54)

The results do show that the resolution functions of X-ray diffractometers are complex and need detailed work to understand each situation because of the non-Gaussian components. Further experimental work should probably be done to eliminate these effects by using multiple-bounce components or by roughening the surfaces of the crystals to reduce the surface streaks. The difficulty with the latter approach is that the process can introduce defects which degrade the resolution and also make the results different from crystal to crystal.

The expert technical assistance of Hugh Vass is very much appreciated. The work was supported by the Science & Engineering Research Council.

References

ANDREWS, S. R. & COWLEY, R. A. (1985). *J. Phys. C*, **18**, 6427-6439.
ANDREWS, S. R. & COWLEY, R. A. (1986). *J. Phys. C*, **19**, 615-635.
BJERRUM-MÖLLER, H. & NIELSEN, M. (1969). In *Proceedings of IAEA Panel Meeting on Instrumentation for Neutrons*. Vienna: IAEA.
COLE, H. & SEMPLE, N. R. (1962). *J. Appl. Phys.* **33**, 2227-2233.
COWLEY, R. A. (1987). *Acta Cryst.* A**43**, 825-836.
COWLEY, R. A. & RYAN, T. (1987). *J. Phys. D.* **20**, 61-68.
GIBBS, D., MONCTON, D. E., D'AMICO, K. L., BOHR, J. & GRIER, B. H. (1985). *Phys. Rev. Lett.* **55**, 234.
GOLDMAN, A. I., MOHANTY, K., SHIRANE, G., HORNE, P. M., GREENE, R. L., PETERS, C. J., THURSTON, T. R. & BIRGENEAU, R. J. (1987). *Phys. Rev. B*, **36**, 5609-5612.
KIKUTA, S. & KOHRA, K. (1970). *J. Phys. Soc. Jpn*, **29**, 1322-1328.
LUCAS, C. (1989). PhD thesis. Edinburgh Univ., Scotland.
LUCAS, C., GARTSTEIN, E. L. & COWLEY, R. A. (1989). *Acta Cryst.* A**45**, 416-422.
PICK, H. A., BICKMANN, K., POFAHL, E., ZWALL, K. & WENZL, H. (1977). *J. Appl. Cryst.* **10**, 450-457.
PYNN, R., FUJII, T. & SHIRANE, G. (1983). *Acta Cryst.* A**39**, 38-46.
RYAN, T. (1986). PhD thesis. Edinburgh Univ., Scotland.
ZACHARIASEN, W. H. (1945). *Theory of X-ray Diffraction in Crystals*. New York: Wiley.
ZAUMSEIL, P. & WINTER, U. (1982). *Phys. Status Solidi A*, **70**, 497-505; **73**, 455-466.